Joint Carrier-Phase Estimation for Digital Subcarrier Multiplexing Systems With Symbol-Rate Optimization

Joint Carrier-Phase Estimation for Digital Subcarrier Multiplexing Systems with Symbol-Rate Optimization

Manuel S. Neves, Andrea Carena, Antonino Nespola, Paulo P. Monteiro and Fernando P. Guiomar

***Abstract*—Digital subcarrier multiplexing (SCM) has recently emerged as a promising solution for next-generation ultra-high-baudrate coherent optical communication systems. Among its distinctive advantages over traditional single-carrier modulation, SCM enables the exploitation of symbol-rate optimization (SRO), which has been shown to enable the passive mitigation of the nonlinear interference noise (NLIN) that is generated during propagation over dispersion-unmanaged optical fiber systems. However, the full exploitation of SRO-based NLIN mitigation is severely hindered by the uncompensated distortion caused by laser phase noise (LPN) and non-linear phase noise (NLPN), whose impact is magnified by the use of low-baudrate subcarriers. Resorting to low-complexity carrier phase estimation (CPE) algorithms, in this paper we experimentally demonstrate that it is possible to overcome the hurdles posed by LPN and NLPN in SCM systems, provided that adequate joint-subcarrier CPE processing is employed. A dual-stage joint-processing approach composed of a pilot-based CPE optionally followed by a blind phase search (BPS)-based estimator is implemented and experimentally assessed, enabling to effectively optimize the symbol-rate per subcarrier down to 3 GBaud, in accordance with the theoretical SRO predictions for the system under test. In addition, we demonstrate that signal-to-noise ratio (SNR) gains of more than 1 dB can be achieved through joint-subcarrier CPE processing in shorter-reach links, while this gain tends to progressively reduce with increasing propagation distance, down to about 0.5 dB gain after 3000 km propagation.**

***Index Terms*—Optical Communications, Coherent Optics, Phase Noise, Carrier Phase Estimation, Subcarrier-Multiplexing, Multicarrier**

I. Introduction

THANKS to the high versatility of their digital signal processing (DSP) units, modern coherent optical systems are nowadays able to support a wide variety of modulation formats and signal transmission paradigms [1]. Notably, the usage of digital subcarrier multiplexing (SCM) modulation has recently gained significant popularity [2]–[5], owing to its prominent advantages when compared to legacy single-carrier systems.

Besides the inherent benefits in terms of practical hardware implementation [5], SCM modulation has also been utilized as a way of mitigating the impact of nonlinear interference noise (NLIN), enabling the so-called process of symbol-rate optimization (SRO) [6], which consists of finding the best symbol-rate per subcarrier that minimizes the generation of NLIN during propagation over a dispersion-unmanaged fiber link. However, the enhanced impact of phase noise on these systems has placed a significant hurdle to the full exploitation of SRO benefits [7]–[9]. In particular, it has been shown that the added non-linear phase noise (NLPN) that is generated during the propagation of high-order QAM signals might be significantly more difficult to mitigate through standard carrier phase estimation (CPE) approaches in SCM systems [9], [10], mainly due to the longer symbol duration associated with the lower symbol-rate per subcarrier. To circumvent this problem, novel joint-subcarrier CPE approaches must be developed and experimentally assessed.

A plethora of diverse CPE approaches has been proposed for coherent optical communications during the last decade. In general terms, CPE can be performed in a data-aided or blind manner, with or without modulation format dependency. Pilot-based CPE is a notorious case of a data-aided and modulation agnostic CPE [11], [12]. By inserting pilot-symbols spread throughout the transmitted signal, the laser phase noise (LPN) can be directly estimated from the phase difference between the sent and received symbols. This technique has been largely adopted in practical applications [13], providing a simple solution to the challenges posed by blind CPE, namely in terms of cycle-slips and phase ambiguity. The extension of pilot-based CPE to SCM systems has already been proposed in [14], as well as to multi-wavelength systems in [15]. On the other hand, blind CPE provides an overhead-free alternative, but at the expense of increased complexity and modulation format-dependency. Some of the most common blind CPE approaches include techniques such as the Viterbi-Viterbi (VV) algorithm [16] or blind phase search (BPS) [17]. Owing to its scalability to higher-order modulation formats, the BPS algorithm has found wide applicability in recent research works [18]. The extension of blind joint-subcarrier CPE in SCM systems has already been proposed in [19] and [20], particularly in [20] an interesting *time-interleaved* approach, in which the transmitted subcarriers are fractionally delayed

This work was partially supported by FEDER, through the CENTRO 2020 program, project ORCIP (CENTRO-01-0145-FEDER-022141), by FCT/MCTES through project FreeComm-B5G (UIDB/EEA/50008/2020), and by the PhotoNext initiative of Politecnico di Torino (http://www.photonext.polito.it/). Fernando P. Guiomar acknowledges a fellowship from "la Caixa" Foundation (ID 100010434). The fellowship code is LCF/BQ/PR20/11770015.

Manuel S. Neves, Paulo P. Monteiro and Fernando P. Guiomar are with Instituto de Telecomunicações, University of Aveiro, 3810-193, Aveiro, Portugal (e-mail: guiomar@av.it.pt)

Andrea Carena is with Dipartimento di Elettronica e Telecomunicazioni, Politecnico di Torino, 10129 Torino, Italy (e-mail: andrea.carena@polito.it)

Antonino Nespola is with LINKS Foundation, via Pier Carlo Boggio 61, 10138 Torino, Italy (e-mail: antonino.nespola@linksfoundation.com)

Manuscript received February XX, 2021; revised March XX, 2021.

to minimize the period between phase estimation instants. In order to combine the advantages of data-aided and blind phase estimation approaches, a dual-stage CPE strategy is often considered in practical applications, consisting of a first low-overhead pilot-based phase estimator, and a second BPS-based CPE to fine-tune the phase compensation [21].

Indeed, several contributions on joint-processing techniques for CPE in SCM systems already exist, as is the case in [14], [19], [20]. However, to the best of our knowledge, a study on experimental results and performance gains in SCM systems was yet to be performed, particularly in terms of the CPE impact in nonlinear regime through symbol-rate optimization. Thus, resorting to offline processing of experimental data obtained from a long-haul polarization-multiplexed 16-*ary* quadrature amplitude modulation (PM-16QAM) transmission system, in this paper we explore the usage of different joint-subcarrier CPE approaches, built upon pilot- and BPS-based phase estimation algorithms. Using legacy single-carrier-like CPE as a baseline performance benchmark, we demonstrate how joint-subcarrier CPE can decisively contribute to fully exploit the theoretically promised SRO gains, while making use of practical and low-complexity phase estimation methods.

The remainder of this paper is structured as follows: in Section II, an introduction to LPN is given and the CPE techniques explored in this work are described; in Section III, the experimental setup is described; in Section IV, the experimental results are presented and discussed; and, finally, in Section V, conclusions are drawn.

II. Laser Phase Noise and Carrier-Phase Estimation

LPN is generally accepted to be modeled as a Wiener process, which is the result of the accumulation of a Gaussian variable, f_i, [17]

$$\phi_{\mathrm{PN}}(k) = \sum_{i=-\infty}^{k} f_i, \tag{1}$$

whose variance, σ_f^2, measured with a sampling period, T_s, is,

$$\sigma_f^2 = 2\pi\Delta f T_s, \tag{2}$$

in which Δf, when neglecting the effects of chromatic dispersion (CD), is the combined laser linewidth (LLW) of both transmitter and local oscillator (LO) lasers (i.e. $\Delta f_{\mathrm{TX}} + \Delta f_{\mathrm{LO}}$). The cumulative nature of ϕ_{PN} in expression (1), leads to a strong time-correlation between phase noise realizations. This important feature of Wiener phase noise is the key to enable its tracking and compensation resorting to proper CPE algorithms.

In the next subsections, we describe two different general approaches to perform CPE in SCM systems, employing subcarrier-independent and joint-subcarrier processing.

A. Subcarrier-Independent CPE

The naive and direct extension of single-carrier pilot-based CPE to SCM systems is to treat and compensate each subcarrier independently. The pilot-symbols are then typically inserted at regularly spaced and aligned positions across all subcarriers, as shown by the red squares (■) in Fig. 1. This approach has the merit of enabling the compensation of uncorrelated phase noises on each subcarrier. However, the Wiener LPN process is known to be frequency-independent, as highlighted by expression (1), and even the impact of NLPN has been shown to have significant correlation between subcarriers [10]. Therefore, the strict assumption of uncorrelated phase noise might be ineffective in typical optical communication systems. On the other hand, the subcarrier-independent processing also shows a major disadvantage: by increasing the number of subcarriers, the symbol period must be likewise increased, and as highlighted by expression (2), the variance – and consequently the impact – of LPN in a system is proportional to the sampling period, T_s. Note that, although the baseline sampling period of the received signal in SCM systems is typically similar to that of single-carrier systems, the CPE stage requires symbol-wise processing, and therefore the sampling period that is effectively visible to the CPE algorithm is equal to the symbol duration of each subcarrier.

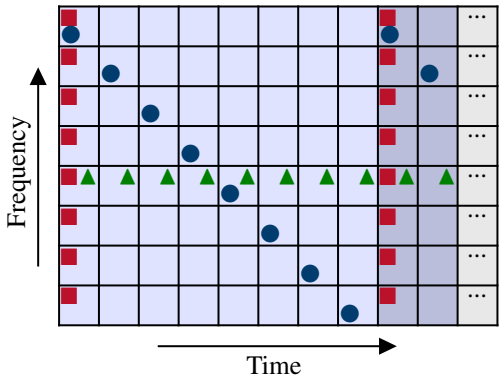

Fig. 1. Frequency/time resource blocks, exemplifying possible allocations for different pilot-based CPE approaches: independent pilots (■), single reference carrier (▲) and spaced pilots (●). Example with $N_{\mathrm{SC}} = 8$ and $R_{\mathrm{P}} = 1/8$ (12.5%).

When employing subcarrier-independent pilot-based CPE, each subcarrier is allocated a number of pilot-symbols, following a ratio, R_{P}, of k/n, in which k is the number of pilot-symbols in every n symbols (payload and pilot-symbols). This first stage of CPE can be followed by a stage of BPS, implemented as described in [17], to improve the tolerance to LPN without additional overhead.

Both the first-stage (pilot-aided) and the second-stage (blind) CPE must typically make use of a moving average window in the LPN estimates, to filter out non-cumulative noise. In the presented results in this manuscript, this moving average is used in both CPE stages. The length of this averaging window is sometimes called the *number of taps*, N_{taps}, of the CPE algorithm, and its optimum value will vary with the amount of noise to which the CPE is subject, as well as with the variance of the Wiener LPN process.

B. Joint-Subcarrier CPE

As opposed to subcarrier-independent CPE, which treats different subcarriers as completely uncorrelated entities, the studied joint-subcarrier carrier phase estimation aims at obtaining a single LPN estimate from the collection of information extracted from each subcarrier, which is then equally applied to compensate all subcarriers. It shall be noted that this approach has an underlying assumption that the noise felt in all the subcarriers is the same, since the goal is to obtain a single LPN estimate. Through joint-subcarrier CPE processing, the frequency of LPN estimation can be improved without requiring an increase of the overall R_{P} or baudrate. Indeed, the ultimate goal of joint-subcarrier CPE is to allow matching the value of T_s in (2) with the corresponding symbol period of an equivalent single-carrier signal, thereby avoiding the penalty associated with the reduction of per-subcarrier baudrate.

First, let us present in detail the several joint-CPE approaches whose performance assessment will be performed in this paper.

1) 1st stage: joint-subcarrier pilot-based CPE: In the first phase estimation stage, we will consider the use of pilot-based CPE, thus benefiting from its advantages in terms of robustness to cycle-slips. In order to optimize this approach to SCM systems, it is critical to make a better use of the existing pilots without modifying the overall R_{P}. Two distinct approaches to do so are suggested in Fig. 1, namely:

- *single reference carrier (SRC)* processing, where all pilot-symbols are inserted into a given reference subcarrier, thereby enabling a minimum time delay between pilot-symbols. For a given pilot-rate, $R_{\mathrm{P}} = 1/n$, with $n \in \mathbb{N}^+$, SRC processing enables a separation of n/N_{SC} symbols between pilot-symbols, where N_{SC} is the number of subcarriers of the SCM signal. In the limit, this strategy corresponds to fully populate the reference subcarrier with pilot-symbols when $n = N_{\mathrm{SC}}$, thus setting the maximum supported pilot-rate for a given SCM signal[1], as depicted in Fig. 1, signaled by green triangles (▲). A similar strategy can be found in [19], treated as "CPE1";
- *spaced pilots (SP)* processing, where the pilot-symbols are evenly spaced among all subcarriers in such a way that the time delay between pilot-symbols is likewise minimized. Again, the minimum inter-pilot-symbols delay, i.e. the existence of consecutive pilot-symbols in every SCM time slot, is achieved with $n = N_{\mathrm{SC}}$, as shown in the example of Fig. 1, signaled by blue circles (●). It shall be noted that this approach implies a pilot-rate $1/n$ such that $n/N_{\mathrm{SC}} \in \mathbb{N}^+$. A similar approach is seen in [14].

The main difference between the SRC and SP implementation of joint-subcarrier pilot-based CPE lies on the origin of the phase noise estimation, which is concentrated on a single subcarrier for the SRC, while it is evenly dispersed among all subcarriers in the SP case. It shall be noted that intermediate approaches can also be considered, namely by selecting a subset of subcarriers to apply the SP strategy. Nevertheless, for the sake of simplicity, in this paper we will focus our analysis on these two exemplary implementation scenarios, SRC and SP.

[1]It is worth referring that, when the maximum pilot-rate is exceeded, i.e. $n < N_{\mathrm{SC}}$, a similar SRC-like strategy can be applied by selecting additional reference subcarriers. Nevertheless, this limit is rarely achieved for typical implementations, and therefore will be neglected in this work.

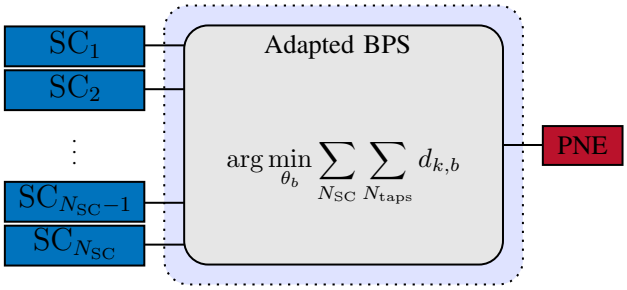

Fig. 2. Demonstrative diagram of the implementation of joint BPS (JBPS). This method achieves a joint phase noise estimate (PNE), that is used to compensate residual LPN in all subcarriers.

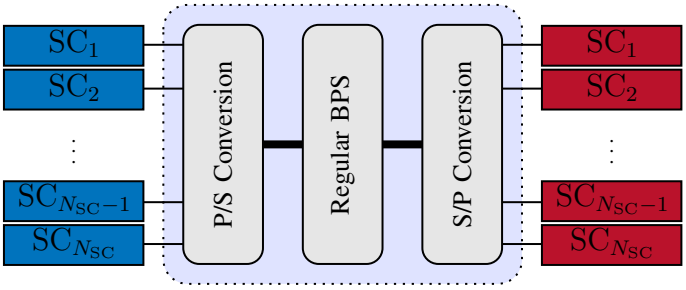

Fig. 3. Demonstrative diagram of the implementation of serialized BPS (SBPS). In this method, the LPN compensation is implicitly performed in the BPS block, prior to the serial-to-parallel conversion.

2) 2nd stage: joint-subcarrier BPS-based CPE: The pilot-based CPE applied in the first stage has the advantage of enabling a robust data-aided estimation of LPN. However, the time resolution of this estimation is also limited by the pilot overhead that is available for that purpose. In most applications, the overhead dedicated to pilot-symbols is not enough to guarantee the aforementioned $n = N_{\mathrm{SC}}$ condition, and therefore the pilot-based phase estimations might be spaced by several symbols. To fill this gap, a second stage blind CPE can be applied to allow for a finer symbol-wise phase estimation. In this work, we will consider two different implementations of BPS-based joint-subcarrier processing:

- *joint BPS (BPS)*, as shown in Fig. 2, which consists of adapting the standard BPS algorithm by extending its averaging process to run not only over N_{taps} in time, but also over N_{SC} subcarriers in frequency. Thereby, instead of N_{SC} independent BPS-based phase estimates, the JBPS yields a single and more noise-tolerant phase noise estimate. A similar strategy can be found in [19], treated as "CPE3";
- *serialized BPS (BPS)*, as depicted in Fig. 3, which consists of applying regular BPS to the received signal, but not without first chronologically serializing the SCM signal, i.e., both the phase-noise estimation and

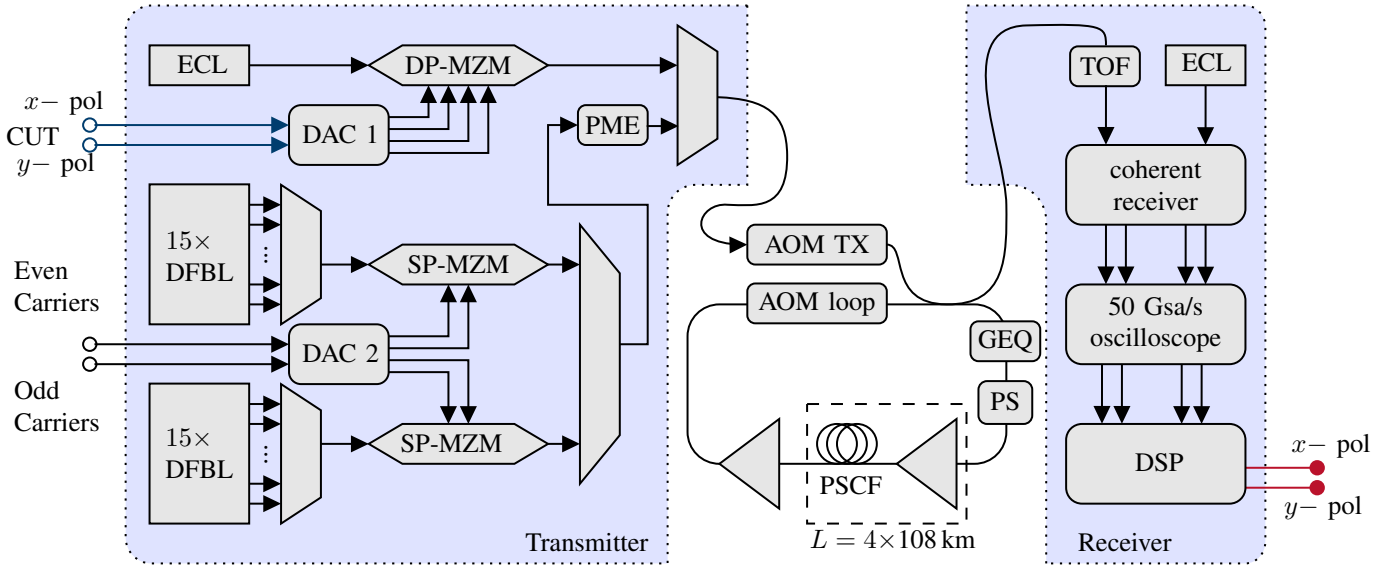

Fig. 4. Experimental setup, as originally presented in [9], utilized to obtain the offline PM-16QAM data (publicly available in an open-access repository [22]), which is hereby reprocessed in this work, employing enhanced joint-subcarrier CPE. In the diagram, we see several building blocks, among which: external cavity laser (ECL), distributed feedback laser (DFBL), digital to analog converter (DAC), dual-pol. (DP-) and single-pol. (SP-) Mach-Zehnder modulator (MZM), polarization multiplexing emulator (PME), acousto-optic modulator (AOM), gain equalizer (GEQ), polarization scrambler (PS), pure silica core fiber (PSCF) and tunable optical filter (TOF)

compensation are performed in the serialized domain. Concerning the signal serialization, it is performed on a per-symbol basis. For each symbol period, one symbol of each subcarrier is taken and appended to the serialized signal, following an order equal to the subcarrier's index $(1, ..., N_{\mathrm{SC}})$. Note that the SBPS processing may benefit from the insertion in the transmitter, in the digital domain, of a time shift among subcarriers equivalent to T_s/N_{SC}, as suggested in [20]. Although this option will not be considered within the course of the experimental assessment performed in this work, this so-called *time-interleaved* BPS variant is deemed relevant only if the symbol period is increased to a point in which significant LPN variations occur within the symbol frame.

III. Experimental Setup

The experimental validation carried out in this paper is based on the offline processing of the data obtained from the experimental setup utilized in the work of [9], which is publicly accessible in an open-access data repository [22].

A. Experimental Setup Configuration

A block diagram depicting the experimental setup is shown in Fig. 4, which consists of 31 co-propagating optical channels, out of which the channel under test (CUT) is the one sitting in the middle, with 15 adjacent channels on each side, in a frequency grid with 28 GHz spacing, centered at 1557.6 nm. All 31 channels are modulated with the same SCM configuration, composed of 2, 4, 8 or 12 subcarriers with 12, 6, 3 or 2 GBaud each, respectively, always adding up to a total of 24 GBaud. The inter-subcarrier frequency spacing is uniform and given by $\Delta f_{\mathrm{SC}} = (1+\alpha)R_s$, with R_s being the subcarrier symbol-rate and $\alpha = 0.05$ the roll-off factor, with exception of the two central subcarriers that have 1 GHz of spacing from the baseband, resulting in a 2 GHz spacing between them. Note that this increased spacing between central subcarriers has been introduced in order to partially avoid the enhanced low-frequency distortion that is generated by the optoelectronic components utilized in the experimental setup. This behavior, commonly identified as the so-called *"M-shape"* performance dependence, has already been reported in several other works employing SCM modulation [23], [24].

At the transmitter, the subcarriers are pulse-shaped by root-raised-cosine (RRC) filter with roll-off factor α and pre-emphasized, accounting for the bandwidth limitations of the digital to analog converters (DACs), operating at 64 GSa/s. The CUT is generated with a dual-polarization Mach-Zehnder modulator (MZM), being the in-phase and quadrature signals for $x-$ and $y-$ polarizations generated by DAC 1, modulating the optical carrier generated by an external cavity laser (ECL) (LLW $<$100 kHz). The other 30 interfering channels are split into odd and even carriers, each light beam is generated by a distributed feedback laser (DFBL) and modulated with a single-polarization MZM and these 30 single-polarization channels are multiplexed and passed through a polarization multiplexing emulator (PME) prior to multiplexing them with the CUT.

The fiber setup is composed of a recirculating loop, to be able to easily monitor the system performance at different transmission lengths, L, with the loop having 4 spans of pure silica core fiber (PSCF) with an average length of 108 km and amplification performed by erbium-doped fiber amplifiers (EDFAs) with a noise figure of 5.2 dB. Additionally, the loop includes a gain equalizer (GEQ) and a polarization scrambler (PS) to average statistically the polarization effects.

Finally, at the receiver, the CUT is filtered by a tunable

optical filter (TOF), mixed with the LO (an ECL, similar to the one on the transmitter), and sampled by a 50 GSa/s real-time oscilloscope (Tektronix DPO73304).

B. Receiver DSP Configuration

The receiver DSP chain can be seen as being composed of three main blocks: i) a pre-CPE DSP subsystem, ii) the CPE subsystem itself and iii) a post-CPE DSP subsystem. In the first block, we perform deskew, chromatic dispersion equalization (CDE), SCM demultiplexing and downsampling (2 samples per symbol), a phase-insensitive 2×2 constant modulus algorithm (CMA) using only 3 taps for coarse subcarrier equalization. Then, standard frequency recovery is applied prior to the CPE subsystem. In the CPE block, we implement either subcarrier-independent CPE or one of the proposed joint-subcarrier techniques. Finally, in the third block, an 8×8 least mean square (LMS) equalizer[2] with 51 taps is used for fine equalization of the subcarriers. Then, downsampling (1 sample per symbol), symbol detection and performance assessment are performed. In the end, a variation of this DSP architecture will also be assessed, in which the 8×8 LMS equalizer is placed between the 1st and 2nd CPE stages. This slight variation aims to assess whether there is a trade-off in the performance of the blind second-stage CPE, between the signal-to-noise ratio (SNR) improvement brought by the equalizer and the phase noise decorrelation among subcarriers due to the phase-sensitive LMS stage. Although it is outside of the scope of this paper, it is worth mentioning that the overall complexity of the DSP stack for SCM systems is known to be comparable or even lower than that imposed by equivalent single-carrier systems [5].

When implementing the CPE approaches, the following relevant implementation details were considered: in pilot-based CPE, interpolation is performed between phase estimates and the pilot-symbols were regular 16-*ary* symbols, since the experimental data was acquired with no particular pilot-symbols allocation; when using SRC, one of the center-most subcarriers was chosen, due to the better SNR and to the fact that this choice of subcarrier minimizes the maximum spectral distance between any other subcarrier and the reference; in terms of BPS-based methods, in all scenarios, the number of test-phases was kept constant, at 16 phases, equally spread over an angle of $\pi/2$.

In all the displayed results, the length of the averaging window in each of the CPE stages was optimized in terms of bit error rate (BER) performance, resorting to a grid-search approach, in which the number of taps was in the range of $[3, 160]$ for pilot-based CPE and $[10, 1500]$ for BPS-based approaches. The elected performance metric was the BER because it is a more intuitive and widespread concept, even though it is known not to be the most theoretically adequate performance metric for these systems, due to the possible paradigm of soft-decision forward error correction (FEC), which makes the relation between post-FEC and pre-FEC become modulation-format-dependent [25]. However, the BER is still meaningful in the context of this manuscript, since the results are compared with the same modulation order and statistical distribution. Furthermore, rather than setting absolute performance limits, the goal of this manuscript is to establish a performance comparison among the tested configurations.

[2]Note that, besides the typical equalization task, the 8×8 equalizer utilized in this work is also targeted to the compensation of residual IQ skew inserted by the transmitter DAC. As shown in [23], the effect of IQ skew in SCM signals generates a spectral mirroring phenomenon that requires the joint equalization of pairs of frequency-symmetric subcarriers, decomposed into their I and Q real-valued components, hence the 8×8 input-output dimensionality. While the complexity of this approach can be reduced in practical applications, e.g. by partially pruning the cross-polarization filters [24], in this work we will consider its full implementation, as originally proposed in [23].

IV. Experimental Results

A. Single-stage CPE

The first step of our experimental analysis will be focused on measuring the impact of symbol-rate optimization of an SCM system while employing legacy subcarrier-independent CPE. With that in mind, Fig. 5.a shows the BER performance associated with the usage of subcarrier-independent pilot-based CPE as a function of the total launch power, for 2, 4, 8, and 12 subcarriers, corresponding to baudrates of 12, 6, 3, and 2 GBaud. The results were extracted for a single circulation (432 km) and $R_{\mathrm{P}} = 1/48$ ($\sim 2\%$). We can observe a significant impact on the BER with the reduction of symbol-rate while using subcarrier-independent pilots. Indeed, while it would be theoretically expectable to observe a minimum BER for this system at approximately 3 GBaud per subcarrier (see [9]), i.e. 8 subcarriers, the best performance provided by subcarrier-independent pilot-based CPE is observed with only 2 subcarriers, then quickly degrading as the subcarrier count increases. This is a clear indication that the lack of CPE accuracy is effectively killing the achievable gains promised by SRO.

Building on these baseline results, but still in the same scenario, let us show what happens to these BER curves if, instead of using subcarrier-independent pilot-based CPE, we evolve to joint-subcarrier CPE, more specifically, to the cases of the already mentioned SRC and SP. The corresponding results are plotted in Figs. 5.b and 5.c, respectively. Analyzing these two figures, it can be seen that indeed collaborative approaches to CPE improve the performance of SCM systems, providing a BER improvement to all tested scenarios. It can be observed that the SRC and SP processing paradigms are nearly matched in terms of performance, with only a marginal advantage to the SRC approach. Moreover, the ever-increasing gap between BER curves in Fig. 5.a is also mitigated, providing to the system a smaller dependency on the elected baudrate. A final observation of interest concerning Figs 5.b and 5.c is that joint-subcarrier CPE reordered the BER curves, with the best performances being achieved for 4 and 8 subcarriers, with baudrates of 6 and 3 GBaud, respectively. It can then be concluded that the use of joint-subcarrier CPE, even in its simplest single-stage and pilot-based implementation, is a key requirement to fully exploit the potential benefits provided by SRO. It is worth noting that in [9] the demonstration of SRO-induced gains was only possible through the use of an

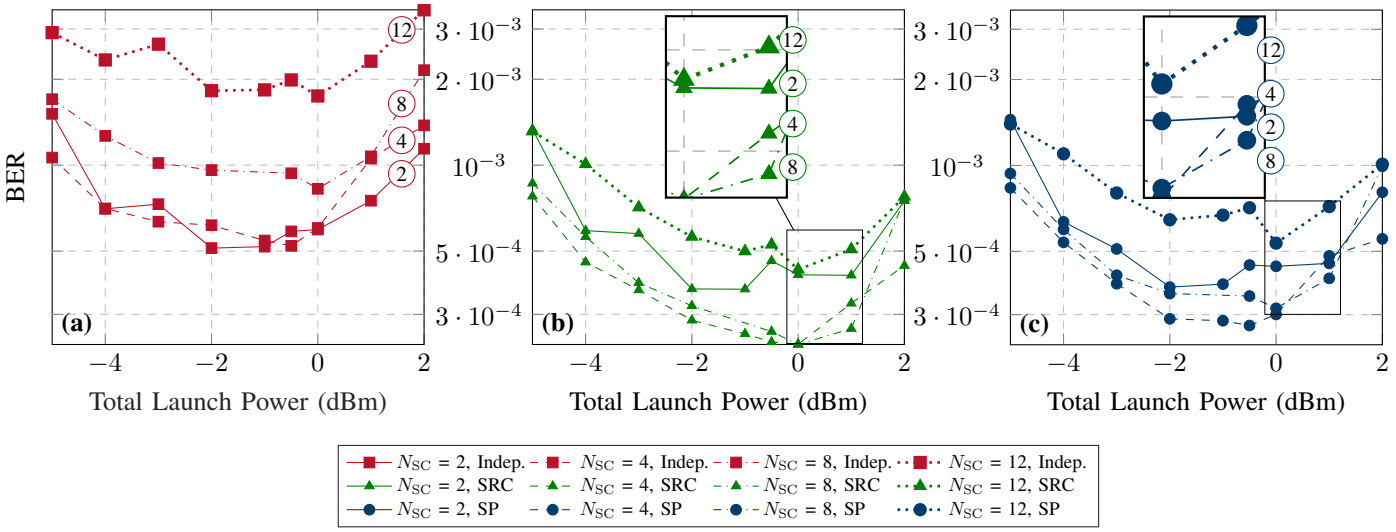

Fig. 5. BER curves as a function of the total launch power for N_{SC}=2, 4, 8, and 12, one circulation (432 km), and $R_P \approx 2\%$, while using **(a)** subcarrier-independent pilot-based CPE, or joint-subcarrier pilot-based CPE, be it **(b)** SRC or **(c)** SP.

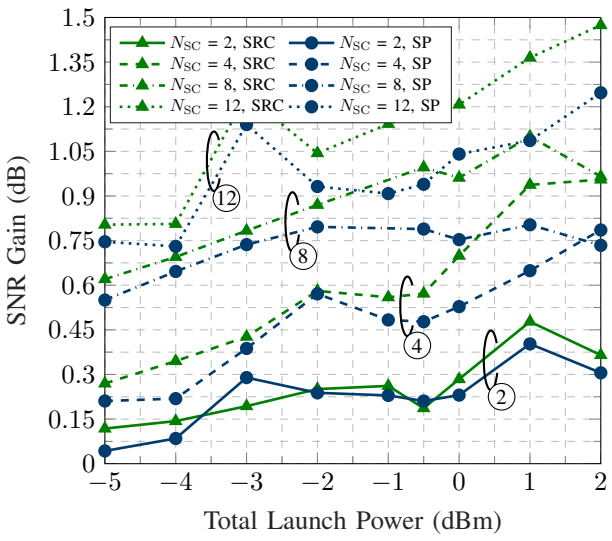

Fig. 6. SNR gain obtained by evolving from subcarrier-independent to joint pilot-based CPE approaches. Results are displayed as a function of the total launch power. $R_P \approx 2\%$ and $L = 432$ km were used.

unrealistic genie-aided CPE (corresponding to a pilot-based implementation with $R_P = 1/1$ (100%)), applied on a per-subcarrier basis. It is therefore notable to observe that the use of joint-subcarrier processing has enabled to reveal the effect of SRO at a very modest pilot-rate of $R_P \approx 2\%$.

The experiments that led to the results in Fig. 5, also led to the results in Fig. 6, which depict the SNR gain from using joint-subcarrier CPE over subcarrier-independent CPE. Note that, in the henceforward presented results, the SNR is calculated from the measured average BER among all subcarriers, applying well-known analytical formulas for 16QAM [3]. From Fig. 6, we are able to draw some interesting conclusions. Even for low subcarrier numbers, like $N_{SC} = 2$, we found the SP and SRC strategies to provide some gain, a gain of up to approximately 0.5 dB for a channel launch power of 1 dBm. Moreover, in all values of N_{SC} a clear tendency was observed, the improvement in the values of BER, and consequently the SNR increased with the launch power, evidencing a robustness to fiber nonlinearities, associated with the finer granularity of LPN estimation achieved through the cooperative CPE in SCM systems. In the conducted experiments, this culminated in a gain of approximately 1.5 dB in the case of $N_{SC} = 12$ and a launch power of 2 dBm, which translates into passing from a BER of 3.5×10^{-3} to one of 7.7×10^{-4}. The results in Fig. 6 also allow to conclude a clear preference on the SRC approach over the SP, being this preference more notable in higher launch powers for higher values of N_{SC}. This performance gap between SRC and SP can be attributed to the fact that SRC has all the pilot-symbols in a reference carrier in the center of the channel, with a better SNR. Therefore, it outperforms SP, which has pilot-symbols equally spread along all the subcarriers instead, including the ones with the worst SNR. This performance difference is not notable for $N_{SC} = 2$, exactly because, in this system, both subcarriers are symmetrical in terms of SNR and thus there is no measurable impact between interpolating between pilot-symbols from different subcarriers or using all pilot-symbols from the same subcarrier. An important conclusion that can be drawn from these results is that, for the considered modulation format, to achieve the overall best BER performance, it is better to sacrifice symbols with better SNR for the insertion of pilot-symbols, even though the pilot-symbols only transmit phase information. It would be interesting to study how these conclusions change if different DSP configurations and higher-order modulation formats are considered, and this study can be addressed in future research.

Henceforward, in most analyses we will focus our attention on the scenario of $N_{SC} = 8$, standing at a baudrate of 3 GBaud, which corresponds to the culprit of SRO gain as demonstrated in [9].

The same performance indicators obtained in Fig. 5 were then reproduced, but now for a total of 5 circulations, adding

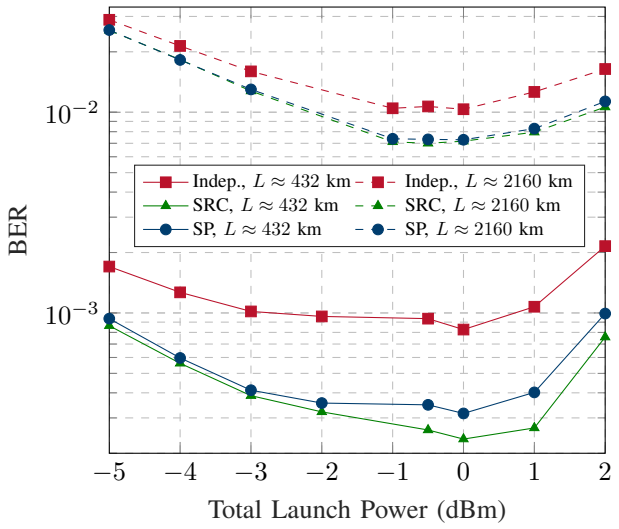

Fig. 7. BER curves as a function of the total launch power for $N_{\mathrm{SC}} = 8$ and $R_{\mathrm{P}} \approx 2\%$, while using both independent and joint approaches. Results for one circulation (432 km, continuous) and 5 circulations (2160 km, dashed).

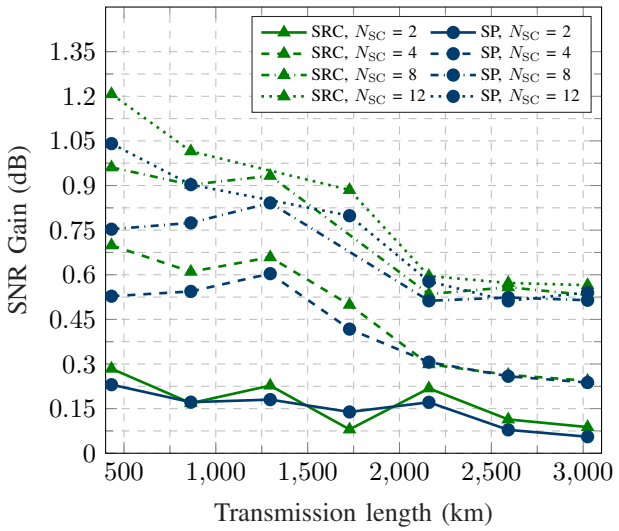

Fig. 8. SNR gain obtained by evolving from subcarrier-independent to joint pilot-based CPE approaches. Results are displayed as a function of the transmission distance. $R_{\mathrm{P}} \approx 2\%$ and a total launch power of 0 dBm were used.

up to a transmission length of approximately 2160 km. These results are shown in Fig. 7, alongside the previous results (for a transmission length of 432 km), for $N_{\mathrm{SC}} = 8$. One remark that can be made concerning these results is that, for $L = 2160$ km, the subcarrier-independent approach did not achieve the BER threshold of 10^{-2}, a typical threshold to allow error-free communication after FEC, while any of the two joint-subcarrier approaches already are able to meet that requirement, for total launch powers in the range of -1 to 1 dBm, thus proving that joint-subcarrier CPE approaches can indeed play a decisive role in SCM systems.

Finally, and under the realization that when passing from $L = 432$ km to $L = 2160$ km, the BER improvement associated with joint-subcarrier techniques decreased, we performed a distance sweep, at a fixed power level of 0 dBm. With this sweep, we intended to assess the SNR gain of the experimented joint approaches when compared to the equivalent subcarrier-independent approach with the increase in the transmission length. We display these results in Fig. 8, where we verify a notorious trend: regardless of the baudrate, joint-subcarrier techniques present a reduced gain as the transmission length increases. The SNR gain degradation is more evident in scenarios that presented larger values of gain for shorter transmission distances, as it is the case for $N_{\mathrm{SC}} = 8$ and $N_{\mathrm{SC}} = 12$. This behavior can be attributed to two main factors at play: i) the reduction of SNR with increasing transmission length, which hinders the task of the CPE in distinguishing between added amplified spontaneous emission (ASE) noise and actual phase noise, and results in wider required moving average windows, and ii) the growing impact of CD with increasing transmission length, which generates a progressive walk-off effect between subcarriers, thereby corrupting the underlying assumption of nearly identical phase noise processes among subcarriers, and undermining the paradigm of the considered joint-subcarrier CPE approaches. In Section IV-B, in the dual-stage CPE analysis, we will assess which of these factors is most responsible for the SNR degradation.

Regarding the optimization of the length of the averaging window on the CPE approaches, N_{taps}, we have found the optimum number to be in the range of [7,59], with an increasing trend as the launch power decreases and the transmission length increases, as expected, given the role of the SNR of the signal on the number of taps. For the case of Fig. 7, at the launch power of 0 dBm, 5 circulations, and 8 subcarriers, the optimum numbers of taps for subcarrier-independent pilot based CPE, SRC, and SP were 11, 39 and 47, respectively. We can verify that joint-subcarrier approaches benefit from higher filtering of the LPN estimates without losing in time resolution thanks to the information from the several subcarriers. The higher number of taps on the SP CPE approach can be attributed to the fact that we have to interpolate among pilot-symbols in the several subcarriers, and thus additional filtering is required, leading to the observed slightly worse performance when compared to SRC CPE.

B. Dual-stage CPE

Let us now proceed with the experimental analysis of the possible improvement enabled by a second stage of CPE, based on the BPS algorithm, following the two approaches introduced in Section II-B: JBPS and SBPS. As our goal is to attain the best achievable CPE performance, we will assume that this is achieved by applying this second stage of joint-subcarrier BPS to the joint-subcarrier implementation of the pilot-based CPE. To keep it a well-grounded comparison, however, we also display the experimental results of a fully independent dual-stage CPE approach, i.e., a first stage of subcarrier independent pilot-aided CPE followed by a second-stage of subcarrier-independent BPS, labeled as “P+BPS”.

Since the second-stage CPE is based on blind approaches that assume all subcarriers to have the same phase noise, we

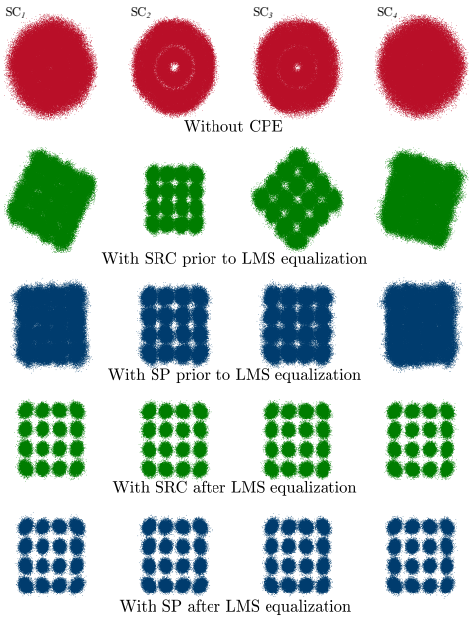

Fig. 9. Constellations after the coarse CMA equalization, before and after the joint-subcarrier pilot-based CPE stage, and also after LMS equalization. Results for $R_{\mathrm{P}} \approx 2\%$, $N_{\mathrm{SC}} = 4$, a launch power of 0 dBm and $L = 432$ km.

should first analyze the signal constellations, and try to infer if this assumption seems correct. To that end, in Fig. 9 we see, for $N_{\mathrm{SC}} = 4$, a launch power of 0 dBm and $L = 432$ km, the resulting constellations before and after the first-stage CPE, and also after the 8×8 LMS equalization. Referring to the constellations after the first CPE stage and before LMS equalization (2nd and 3rd rows in Fig. 9), it can be observed that, as of now, only the SP approach would be fit for a second-stage of joint-subcarrier BPS, since SRC leaves behind a constant rotation in all subcarriers except for the reference subcarrier, due to small offsets in the static chromatic dispersion equalization. However, this constant phase rotation is easily corrected with negligible pilot-symbols allocation.

In contrast, after the phase-sensitive LMS equalization, it can be seen that not only the SNR is significantly improved, but also all subcarriers are properly aligned, both with SP and SRC, enabling the seamless application of a second-stage BPS-based CPE. Based on these observations, in the following experimental analysis we will consider two alternative DSP implementations:

i) pilot-based CPE $\rightarrow$ BPS-based CPE $\rightarrow$ LMS equalizer;
ii) pilot-based CPE $\rightarrow$ LMS equalizer $\rightarrow$ BPS-based CPE.

Employing DSP strategy i), two pairs of results are shown, both showcasing the results obtained with the studied second-stage BPS-based CPE approaches: Figs. 10.a and 11.a represent a launch power sweep for a transmission length of 432 km and a transmission length sweep for a launch power of 0 dBm, respectively, both for the case in which SP was considered as the first-stage CPE; and Figs. 10.b and 11.b represent the same as the previous pair, but now considering SRC as the first-stage CPE. The constant experimental parameters are the number of subcarriers, 8, and the overall pilot-rate, $\sim$2%. We can observe that, as expected, applying blind CPE stage prior to the LMS equalization leads to a severe penalty on the performance of the regular (subcarrier-independent) BPS, resulting in a performance degradation over any of the single-stage joint-subcarrier CPE for most evaluated scenarios. As for the blind joint-subcarrier approaches to the second-stage CPE, first, analyzing the scenario with SP as a first-stage CPE, in Figs. 10.a and 11.a both resulted in an improvement in the system performances over the single-stage CPE, with the SBPS approach resulting in a better performance over the JBPS approach. The SNR gains associated with the application of joint-subcarrier BPS over the baseline subcarrier-independent BPS are considerable: up to 0.4 dB at the optimum launched power, and this proves that blind approaches can also benefit from joint-subcarrier CPE approaches, provided that it is guaranteed that the LPN affecting all subcarriers is correlated (in this case, by having a first-stage CPE based on a joint-subcarrier method). For DSP strategy i), the fully subcarrier-independent dual-stage CPE results are not displayed because they do not present any advantage over the same results in DSP strategy ii). Now, analyzing the scenario with SRC as a first-stage CPE, in Figs. 10.b and 11.b, it is observed that, with this DSP strategy, the SRC approach does not leave much margin for performance improvement for the second-stage BPS-based CPE, since only the SBPS approach presented a marginal gain of 0.05 dB in some cases of interest.

Employing DSP strategy ii), Figs. 10.c and 11.c, and Figs. 10.d and 11.d show the same results as in Figs. 10.a and 11.a, and Figs. 10.b and 11.b, respectively, but now with the second-stage CPE applied after the LMS equalization, having either SP or SRC as a first stage CPE. These figures also feature the curves of fully subcarrier-independent dual-stage CPE, which are of interest in this DSP strategy. The results show that equalization is undoubtedly an important requirement prior to blind equalization, enabling to achieve significant gains over the single-stage CPE. It is also worth noting that these BPS-induced gains are clearly correlated with the increase of optical launched power, achieving up 0.8 dB SNR gain at 2 dBm. This shows that the second-stage BPS-based CPE plays an important role in the mitigation of NLPN, as it enables a finer time resolution for phase estimation. However, it is worth noting that the intermediate LMS equalization stage can be reducing part of the gain of joint-subcarrier BPS approaches (only about 0.1 dB in the best cases), since its phase-sensitive equalization contributes to partially decorrelate the phase noise processes between subcarriers. In summary, although it is generally preferable to include a fine equalization stage before the second-stage blind CPE, its inclusion is also a limiting aspect for the exploitation of blind joint-subcarrier CPE processing. In this sense, the development of novel algorithms for collaborative equalization and phase estimation supporting joint-subcarrier processing, might be an important step forward that should be addressed in future research.

To conclude, let us now analyze the performance of the fully subcarrier-independent dual-stage CPE, labeled as "P+BPS" in (c) and (d) of Figs. 10 and 11. There are three main relevant observations to be made concerning these curves. The first is that, when considering regular BPS, a reasonably constant

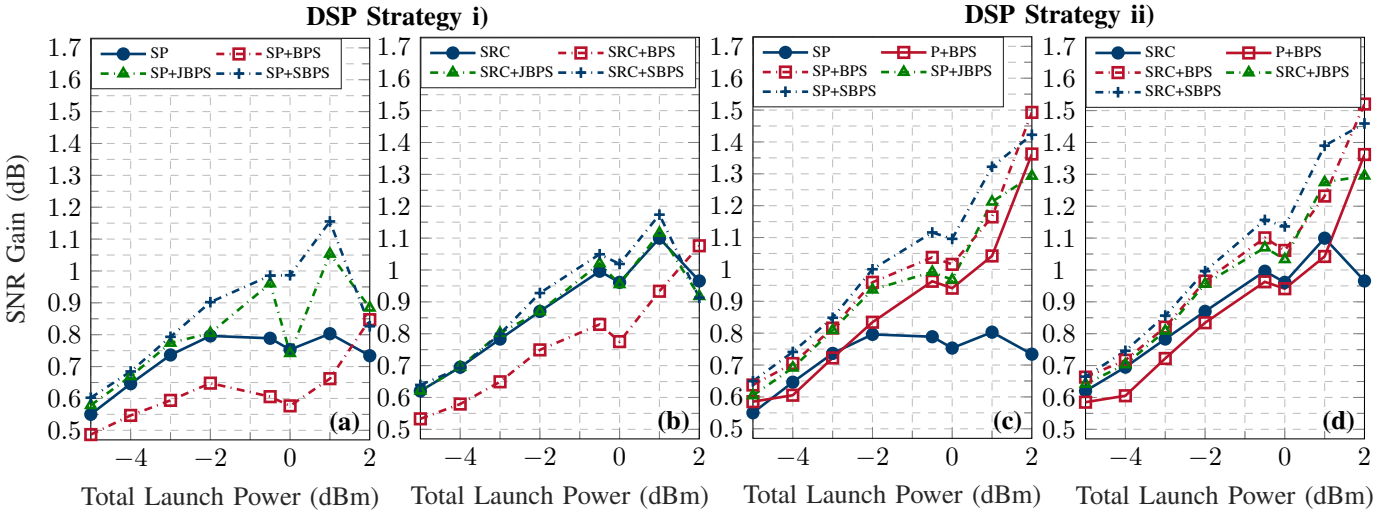

Fig. 10. SNR gain obtained by evolving from single-stage subcarrier-independent pilot-based CPE to joint dual-stage CPE approaches. Results are presented as a function of the total launch power for $N_{\mathrm{SC}} = 8$, one circulation (432 km) and $R_{\mathrm{P}} \approx 2\%$, having as first-stage CPE: **(a)** the SP, **(b)** the SRC, **(c)** the SP and LMS prior to the second-stage CPE, and **(d)** the SRC and LMS prior to the second-stage CPE. Additionally, in **(c)** and **(d)**, results for the fully subcarrier-independent dual-stage CPE are presented for comparison (P+BPS).

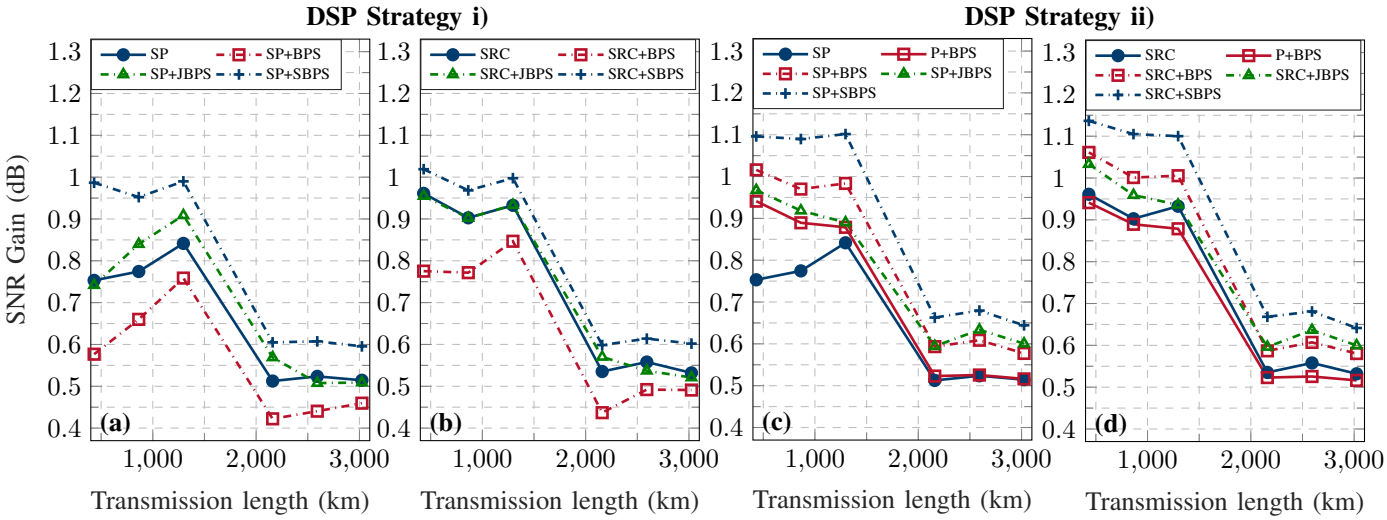

Fig. 11. SNR gain obtained by evolving from single-stage subcarrier-independent pilot-based CPE to joint dual-stage CPE approaches. Results are presented as a function of the transmission distance. And for $N_{\mathrm{SC}} = 8$, a $R_{\mathrm{P}} \approx 2\%$ and a total launch power of 0 dBm, having as first-stage CPE: **(a)** the SP, **(b)** the SRC, **(c)** the SP and LMS prior to the second-stage CPE, and **(d)** the SRC and LMS prior to the second-stage CPE. Additionally, in **(c)** and **(d)**, results for the fully subcarrier-independent dual-stage CPE are presented for comparison (P+BPS).

offset of approximately 0.1 dB was observed when passing from a subcarrier-independent (P+BPS) to a joint-subcarrier (SP/SRC+BPS) first-stage CPE . The second is that the SNR degradation with the transmission length increase was equally felt in this subcarrier-independent approach as it was in the joint-subcarrier methods, thus meaning that, in the assessed scenario, the factor responsible for the SNR gain degradation of the joint-subcarrier CPE techniques with the transmission length increase is mostly driven by the accumulation of ASE noise and subsequent reduction of SNR. Finally, the third observation is that, focusing our attention on Figs. 10.d and 11.d, for most analyzed scenarios a joint-subcarrier single-stage CPE outperforms a subcarrier-independent dual-stage CPE, and this is a remarkable conclusion because the same performance is achieved with a significant reduction on the system's complexity.

As done in the Section IV-A, let us now comment on the optimization of the length of the averaging window on the CPE approaches, N_{taps}, but now regarding the studied second-stage approaches. We have found the optimum number to be in the range of [11,101]. As an example, for the particular case of a launch power of 0 dBm, a transmission length of 432 km, and 8 subcarriers, using DSP Strategy ii), the optimum values of N_{taps} were 21 for P+BPS scenario, 41 for SRC+BPS, 11 for SRC+JBPS, 21 for SRC+SBPS, 21 for SP+BPS, 11 for SP+JBPS, and 21 for SP+SBPS. It shall be noted that the smaller number of taps required by the JBPS approach when compared to the SBPS is expected, due to the additional

filtering resulting from the averaging over the number of subcarriers, which is not accounted for in the number of taps.

V. Conclusions

In this paper an experimental assessment of the performance of low-complexity joint-subcarrier CPE approaches in SCM systems was performed, resorting to a combination of two stages of CPE: a first low-overhead pilot-based stage and a second BPS-based stage. It was experimentally shown that the SNR gain from the application of joint-subcarrier CPE approaches increases with the total launch power of the system, demonstrating its effective capability to track and compensate for NLPN distortions, and thereby unlocking the benefits of SRO-based nonlinear mitigation: enabled by joint-subcarrier processing with a pilot overhead of only 2%, an optimum symbol-rate of 3 GBaud per subcarrier was achieved, a major improvement over the 12 GBaud per subcarrier required by legacy subcarrier-independent CPE. Alternatively, if aiming at low-complexity SCM systems, single-stage joint-subcarrier CPE was shown to outperform dual-stage subcarrier-independent CPE. Furthermore, the impact of phase-sensitive equalization on the effectiveness of joint-subcarrier blind CPE has been addressed, exposing a tradeoff between improved overall performance and degraded joint-subcarrier processing.

References

[1] G. Bosco, "Advanced modulation techniques for flexible optical transceivers: the rate/reach trade-off," *Journal of Lightwave Technology*, vol. 37, no. 1, pp. 36–49, 2018.

[2] M. Qiu, Q. Zhuge, M. Chagnon, Y. Gao, X. Xu, M. Morsy-Osman, and D. V. Plant, "Digital subcarrier multiplexing for fiber nonlinearity mitigation in coherent optical communication systems," *Opt. Express*, vol. 22, no. 15, pp. 18 770–18 777, 2014.

[3] F. P. Guiomar, L. Bertignono, A. Nespola, and A. Carena, "Frequency-domain hybrid modulation formats for high bit-rate flexibility and nonlinear robustness," *Journal of Lightwave Technology*, vol. 36, no. 20, pp. 4856–4870, 2018.

[4] A. Kumpera, V. Dominic, A. Awadalla, L. Dardis, J. Rahn, S. Sanders, M. Mitchell, P. Mertz, G. Shartle, S. Jackson, S. Blakey, M. Sokar, D. Krause, H. Sun, K.-T. Wu, and P. Cannon, "Real-time superchannel transmission over 10,500 km submarine link at 4.66 b/s/Hz spectral efficiency," *Opt. Express*, vol. 26, no. 12, pp. 15 039–15 044, Jun 2018.

[5] H. Sun, M. Torbatian, M. Karimi, R. Maher, S. Thomson, M. Tehrani, Y. Gao, A. Kumpera, G. Soliman, A. Kakkar, M. Osman, Z. A. El-Sahn, C. Doggart, W. Hou, S. Sutarwala, Y. Wu, M. R. Chitgarha, V. Lal, H. Tsai, S. Corzine, J. Zhang, J. Osenbach, S. Buggaveeti, Z. Morbi, M. Iglesias Olmedo, I. Leung, X. Xu, P. Samra, V. Dominic, S. Sanders, M. Ziari, A. Napoli, B. Spinnler, K. Wu, and P. Kandappan, "800G DSP ASIC design using probabilistic shaping and digital sub-carrier multiplexing," *Journal of Lightwave Technology*, vol. 38, no. 17, pp. 4744 – 4756, 2020.

[6] P. Poggiolini, A. Nespola, Y. Jiang, G. Bosco, A. Carena, L. Bertignono, S. M. Bilal, S. Abrate, and F. Forghieri, "Analytical and experimental results on system maximum reach increase through symbol rate optimization," *J. Lightw. Technol.*, vol. 34, no. 8, pp. 1872–1885, April 2016.

[7] J. X. Cai, M. Mazurczyk, O. V. Sinkin, M. Bolshtyansky, D. G. Foursa, and A. Pilipetskii, "Experimental study of subcarrier multiplexing benefit in 74 nm bandwidth transmission up to 20,450 km," in *Proc. European Conference on Optical Communication (ECOC)*, 2016, pp. 677–679.

[8] A. C. Meseguer, J. Renaudier, R. Rios-Müller, P. Tran, and G. Charlet, "Impact of bandwidth efficiency in nonlinear tolerance of multicarrier modulations," *J. Lightwave Technol.*, vol. 34, no. 8, pp. 1787–1792, April 2016.

[9] F. P. Guiomar, A. Carena, G. Bosco, L. Bertignono, A. Nespola, and P. Poggiolini, "Nonlinear mitigation on subcarrier-multiplexed PM-16QAM optical systems," *Opt. Express*, vol. 25, no. 4, pp. 4298–4311, Feb 2017.

[10] O. Golani, D. Pilori, F. P. P. Guiomar, G. Bosco, A. Carena, and M. Shtaif, "Correlated nonlinear phase-noise in multi-subcarrier systems: Modeling and mitigation," *Journal of Lightwave Technology*, vol. 38, no. 6, pp. 1148–1156, mar 2020.

[11] M. Magarini, L. Barletta, A. Spalvieri, F. Vacondio, T. Pfau, M. Pepe, M. Bertolini, and G. Gavioli, "Pilot-symbols-aided carrier-phase recovery for 100-G PM-QPSK digital coherent receivers," *IEEE Photon. Technol. Lett.*, vol. 24, no. 9, pp. 739 –741, may1, 2012.

[12] M. Mazur, J. Schröder, A. Lorences-Riesgo, M. Karlsson, and P. A. Andrekson, "Optimization of low-complexity pilot-based DSP for high spectral efficiency 51×24 GBaud PM-64QAM transmission," in *Proc. European Conf. Optical Communication (ECOC)*, Sep. 2018.

[13] E. Borjeson, C. Fougstedt, and P. Larsson-Edefors, "VLSI implementations of carrier phase recovery algorithms for M-QAM fiber-optic systems," *Journal of Lightwave Technology*, vol. 38, no. 14, pp. 3616–3623, jul 2020.

[14] M. P. Yankov, L. Barletta, and D. Zibar, "Phase noise compensation for nonlinearity-tolerant digital subcarrier systems with high-order QAM," *IEEE Photonics Journal*, vol. 9, no. 5, pp. 1–12, 2017.

[15] A. F. Alfredsson, E. Agrell, M. Karlsson, and H. Wymeersch, "Pilot distributions for joint-channel carrier-phase estimation in multichannel optical communications," *Journal of Lightwave Technology*, vol. 38, no. 17, pp. 4656–4663, sep 2020.

[16] A. Viterbi, "Nonlinear estimation of PSK-modulated carrier phase with application to burst digital transmission," *IEEE Transactions on Information Theory*, vol. 29, no. 4, pp. 543–551, 1983.

[17] T. Pfau, S. Hoffmann, and R. Noé, "Hardware-efficient coherent digital receiver concept with feedforward carrier recovery for M-QAM constellations," *J. Lightwave Technol.*, vol. 27, no. 8, pp. 989–999, Apr 2009.

[18] X. Yan, C. Cao, W. Zhang, X. Zeng, Z. Feng, Z. Wu, X. Su, and T. Wang, "Low-complexity carrier phase estimation for M-ary quadrature amplitude modulation optical communication based on dichotomy," *Optics Express*, vol. 28, no. 17, p. 25263, aug 2020.

[19] S. M. Bilal, C. Fludger, and G. Bosco, "Carrier phase estimation in multi-subcarrier coherent optical systems," *IEEE Photonics Technology Letters*, vol. 28, no. 19, pp. 2090–2093, 2016.

[20] D. Martinez, Y. Mori, H. Hasegawa, and K. ichi Sato, "Novel subcarrier multiplexing and subcarrier-synchronous phase estimation tolerant to laser phase noise," in *Advanced Photonics, Signal Processing in Photonic Communications (SPPCom)*, 2017, p. SpW1F.5.

[21] X. Zhou, L. E. Nelson, P. Magill, R. Isaac, B. Zhu, D. W. Peckham, P. I. Borel, and K. Carlson, "High spectral efficiency 400 Gb/s transmission using PDM time-domain hybrid 32–64 QAM and training-assisted carrier recovery," *Journal of Lightwave Technology*, vol. 31, no. 7, pp. 999–1005, apr 2013.

[22] F. Guiomar and A. Carena, "Experimental data on PM-16QAM long-haul transmission (after DSP)," 2019. [Online]. Available: https://doi.org/10.5281/ZENODO.2581091

[23] G. Bosco, S. M. Bilal, A. Nespola, P. Poggiolini, and F. Forghieri, "Impact of the transmitter IQ-skew in multi-subcarrier coherent optical systems," in *Proc. Optical Fiber Communication Conf. and Exposition (OFC)*, 2016, p. W4A.5.

[24] S. Ziaie, F. P. Guiomar, N. J. Muga, A. Nespola, G. Bosco, A. Carena, and A. N. Pinto, "Adaptive Stokes-based polarization demultiplexing for long-haul multi-subcarrier systems," *IEEE Photonics Technology Letters*, vol. 31, no. 10, pp. 759–762, 2019.

[25] A. Alvarado, E. Agrell, D. Lavery, R. Maher, and P. Bayvel, "Replacing the soft-decision FEC limit paradigm in the design of optical communication systems," *Journal of Lightwave Technology*, vol. 34, no. 2, pp. 707–721, 2016.